



# Groundwater flow system understanding of the lukewarm springs in Kistapolca (South Hungary) and its relevance to hypogene cave formation

Anita Eröss<sup>1</sup> · Katalin Csondor<sup>1</sup> · György Czuppon<sup>2,4</sup> · József Dezső<sup>3</sup> · Imre Müller<sup>1</sup>

Received: 14 June 2019 / Accepted: 18 February 2020 / Published online: 5 March 2020  
© The Author(s) 2020

## Abstract

Springs have an important role both in groundwater flow system understanding and in maintaining groundwater-related ecosystems. The aim of the research of the lukewarm karst springs in Kistapolca is to understand the origin of the elevated temperature (22–24 °C), i.e., whether it is the result of mixing of cold and thermal waters or it represents the terminal area of intermediate flow systems. This question has also an important relevance to the evaluation of recent cave formation in the area. In case of mixing of different waters dissolution by mixing corrosion could take place. This scenario was proposed for the formation of the Beremend Cave, which is situated in the close vicinity of the springs, and which is the only known cave of the area, where the passages are partly filled by water. Therefore, several methods, including geophysical, geochemical and stable isotope measurements, evaluation of continuous-time series of water level change, temperature, and electrical conductivity data and hydraulic evaluation of vertical flow conditions by pressure–elevation profiles were combined in order to acquire information about the hydrogeological environment and flow conditions in the area. The results show that a higher order flow system derived from the Villány Hills feeds the springs in Kistapolca without significant local influence. In addition, the results related to the Beremend Cave indicate that cave formation by mixing corrosion is not an active process today in the area, the cave is rather influenced by local processes.

**Keywords** Lukewarm spring · Mixing · Karst · Groundwater flow system · Groundwater-dependent ecosystem · Cave

---

This article is a part of the Topical Collection in Environmental Earth Sciences on “Mineral and Thermal Waters” guest edited by Drs. Adam Porowski, Nina Rman and Istvan Forizs, with James LaMoreaux as the Editor-in-Chief.

---

✉ Anita Eröss  
anita.eross@geology.elte.hu

<sup>1</sup> József and Erzsébet Tóth Endowed Hydrogeology Chair, Department of Geology, Institute of Geography and Earth Sciences, Faculty of Science, Eötvös Loránd University, Pázmány Péter sétány 1/c, 1117 Budapest, Hungary

<sup>2</sup> Institute for Geological and Geochemical Research, Budaörsi Str. 45, 1112 Budapest, Hungary

<sup>3</sup> Institute of Geography and Earth Sciences, University of Pécs, Ifjúság Str. 6, 7624 Pécs, Hungary

<sup>4</sup> Department of Hydrogeology and Engineering Geology, Institute of Environmental Management, University of Miskolc-Campus, 3515 Miskolc, Hungary

## Introduction

Springs are the surface manifestations of groundwater flow systems (Tóth 1971). Their appearance and physicochemical parameters represent the flow system as a whole and report on the rock–water interactions along the flow path. Nowadays most of the springs lost their natural character, because of anthropogenic influence, i.e., they are captured and intensely used. Therefore, the rather rare natural springs are of great importance to study the flow system of an area (Groves 2007). Moreover, natural springs usually maintain groundwater-dependent ecosystems in forms of creeks, lakes, wetlands, etc., which also emphasizes their value.

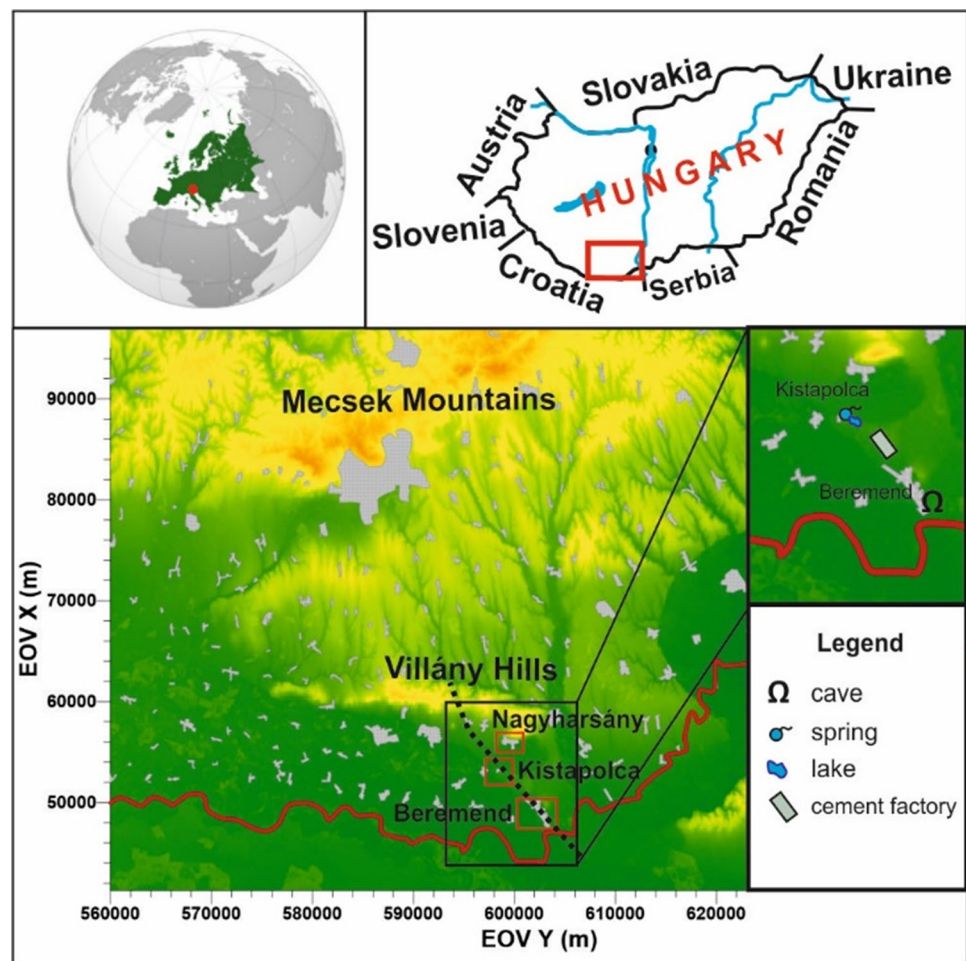
Lukewarm springs are characterized by slightly higher temperatures than the average annual air temperature, but considerably lower than the human body temperature (Meinzer 1923; Pentecost et al. 2003). They represent either a discharge of intermediate flow systems or a mixture of waters with different temperatures derived from different order flow systems. If the latter case takes place

in a carbonate rock environment, the mixing process can lead to the “mixing corrosion” phenomenon (Bögli 1964, 1980) resulting in carbonate dissolution, i.e., cave formation, because the waters present in this process are also characterized by different chemical composition ( $\text{CO}_2$  content) beside the different temperature. Mixing corrosion is a common cave forming process in hypogene karst areas, which are typical for regional discharge areas of karstic groundwater flow systems. To these areas different order flow systems convey waters with different temperatures and geochemical composition. One of the well-known examples for such situation is the hypogene karst system in Budapest (Hungary) (Erőss et al. 2012; Leél-Őssy 2017; Mádl-Szőnyi et al. 2017). Moreover, there are many other areas where recent thermal or lukewarm waters and caves are associated (Bakalowicz et al. 1987; Plan et al. 2006, 2012; Spötl et al. 2009; Dublyansky et al. 2017). The cave morphologies and the mineral assemblages often reflect clearly the effects of upward flowing waters with elevated temperatures (Palmer 2007; Klimchouk 2012; Leél-Őssy 2017).

The karst springs in the little village of South Hungary, Kistapolca (Fig. 1), are captured, but the only naturally

outflowing springs in the Villány karst area nowadays. Their temperatures are about 22–24 °C, well above the annual mean temperature (11 °C). Previous studies by Rónaki et al. (1967) and Lorberer and Rónaki (1978) suggested that the lukewarm temperature is the result of mixing between thermal and cold karst waters. To investigate this question is of great importance since only 6 km away from Kistapolca can be found one of the most protected hypogene caves of Hungary, the Beremend Cave (Fig. 1), which still have underwater passages. The morphology and the minerals decorating the cave walls indicate the effect of thermal waters (Takács-Bolner 1985, 2003a; Vigassy et al. 2010). The question can be raised whether the lukewarm spring water temperature is the result of mixing, and whether this mixing together with the resulting cave formation is active even today, in the recent hydrogeological settings. Since understanding of karstification requires clarifying the groundwater flow conditions in an area (Klimchouk 2007, 2012), these questions can be answered by studying the only natural lukewarm springs and its hydrogeological background in the vicinity, i.e., in Kistapolca.

**Fig. 1** Location of the study area in South Hungary. Dotted line indicates the profile of the 2D numerical model



The springs in Kistapolca also maintain a lake, which has been dried up several times in the last few years. Flow system understanding can also help to explore the reason of these dry periods and constrain the mechanism, as groundwater-dependent ecosystems maintained by the different order flow system’s discharge react differently to climatic changes or anthropogenic effects (Havril et al. 2018).

The aim of the study is to explore the hydrogeological characteristics of the Kistapolca area in order to (1) understand the origin of the elevated temperature; (2) to analyze its relevance to hypogene cave formation; and (3) to evaluate the vulnerability of the lake in Kistapolca as a groundwater-dependent ecosystem maintained by the springs.

### Geological and hydrogeological background

Kistapolca is located in the southern foreground of the Villány Hills, in the south-western part of the Pannonian Basin in Hungary (Fig. 1). The 30 km long Villány Hills is built up by various Mesozoic carbonates (Vadász 1935; Nagy

and Nagy 1976; Török 1998). The carbonate rocks continue in the foreland basin basement, where they are covered by young sediments (Fig. 2). The whole carbonate rock suite forms a thick (up to 1700 m) karst reservoir. The younger cover sediments of Miocene, Pliocene, Pleistocene age consist of sand, clayey silt and loess, which form 0–450 m cover above the carbonate aquifer with alternating aquifer/aquitard characteristics in the surroundings of Kistapolca (Deák et al. 1969). Due to the Late Cretaceous nappe formation, which created the seven structural imbrications of the Mesozoic carbonates (Császár 2002; Petrik 2009; Konrád et al. 2010) (Fig. 2), some basement carbonate outcrops can be also found in the southern foreland of the Villány Hills on or close to the surface. Kistapolca is situated at one of these situations (Fig. 2).

Such marginal areas of outcropping carbonates and sedimentary basins with the same carbonate rock basement are favorable sites for the development of hypogene caves (Mádl-Szőnyi et al. 2017). In the 10 km surroundings of Kistapolca, there are two hypogene caves, in Nagyharsány and Beremend (Fig. 2). These caves are characterized by

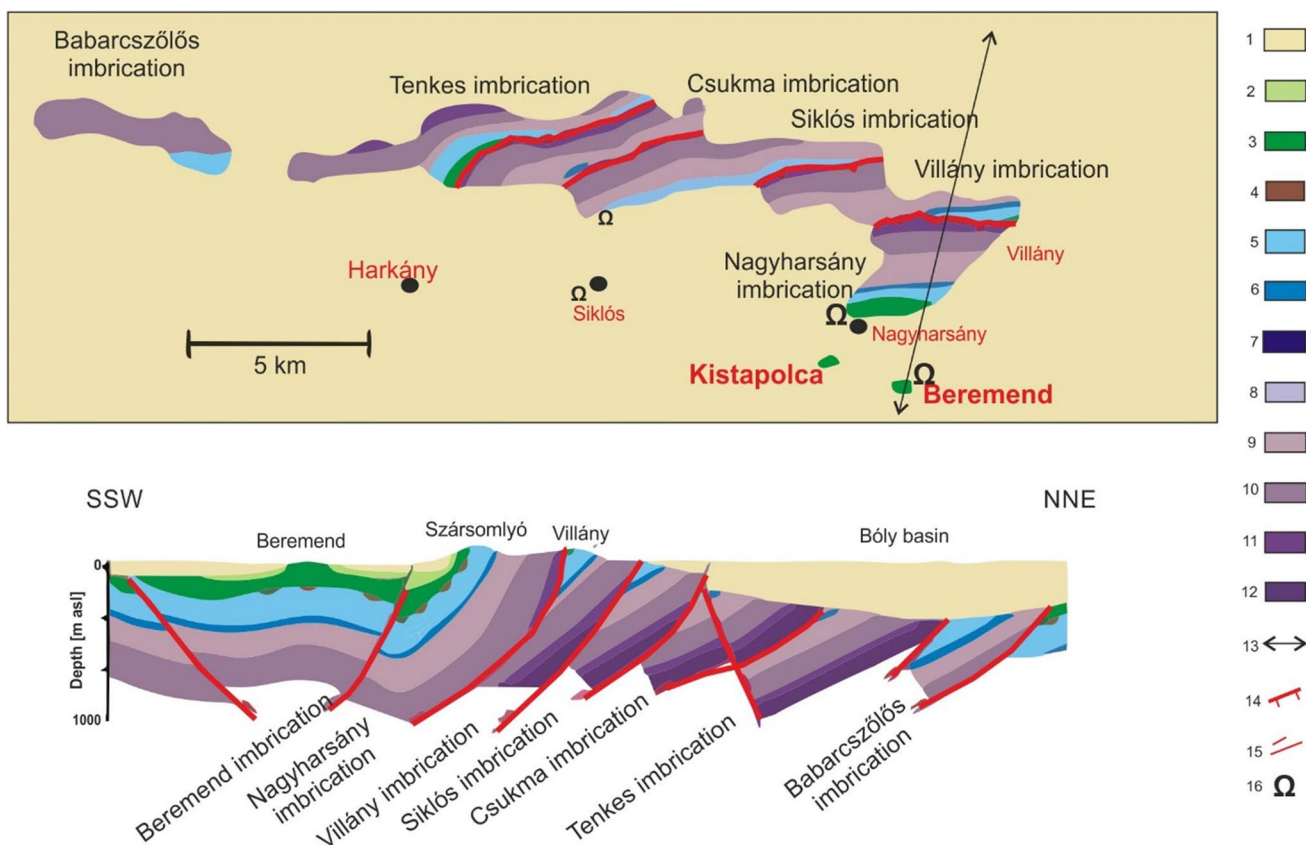


**Fig. 2** Schematic geological build-up of the Villány Hills area (modified after Dezső et al. 2004; Rakusz and Strauss 1953). 1 Neogene sediments; 2 Upper-Cretaceous marl; 3 Lower-Cretaceous marl; 4 Lower-Cretaceous bauxite; 5 Upper-Jurassic limestone; 6 Middle-Jurassic ammonitic limestone; 7 Lower-Jurassic sandy limestone;

8 Upper-Triassic limestone; 9 Middle-Triassic dolomite; 10 Middle-Triassic limestone; 11 Middle-Triassic multi-colored dolomite; 12 Middle-Triassic mudstone; 13 track of the 2D cross-section; 14 imbrication boundary; 15 thrust; 16 cave

phenomena that can be related to the influence of thermal water (Takács-Bolner 1985; Takács-Bolner 2003a, b; Vigassy et al. 2010). Recently, only the Beremend Cave has connection to the karst aquifer, as it has underwater cave passages.

Liebe and Lorberer (1981) described the groundwater flow system in the Villány area as gravity and temperature (density)-difference driven flow system, where on the surface of bare carbonates (i.e., in the Villány Hills) infiltrating meteoric waters circulate and discharge in karst springs with different temperatures. However, they called attention to the possibility of other water components because according to their investigations in the Villány Hills infiltrating meteoric waters can sustain only the lukewarm springs' discharge. Therefore, they suggested connection possibilities of the carbonate reservoir with other deep aquifer units. In the case of the lukewarm springs in Kistapolca, Lorberer and Rónaki (1978) proposed that the cold karst waters originate from direct infiltration in the Villány Hills, and the thermal component is derived from the SW. Csicsák and Gondár (2008) suggested the effect of tectonic compression- and compaction-driven fluid flow from the South, from the sedimentary layers of the Drava Basin (part of the Pannonian Basin). Based on trace element measurements (Scheuer 2012), active tectonics induced mantle fluid contribution may also play a role in the geochemical composition of thermal waters.

The Kistapolca area was subject of intense research in the 1950s and 1960s for water supply purposes of the cement factory (Fig. 1). In the framework of this research, geoelectric measurements were conducted to target the uplifted carbonate basement blocks (Rónaki et al. 1967; Deák et al. 1969). In addition, two springs were captured with 8–12 l/s discharge (Kessler 1959; Rónaki et al. 1967), which fed the lake in Kistapolca. Lorberer and Rónaki (1978) have already mentioned the possible effect of the cement factory due to planned intense water abstraction on the springs' discharge by this time.

## Methods

To explore the hydrogeological characteristics of the Kistapolca area different techniques, including geophysical, geochemical, and stable isotope measurements, evaluation of continuous-time series of water level, temperature, and electrical conductivity data and hydraulic evaluation of vertical flow conditions by pressure–elevation profiles were combined.

Since the appearance of the springs in Kistapolca is thought to be connected to an uplifted carbonate basement block, geophysical methods were applied first to investigate this question in detail. Pressure–elevation profiles were

constructed based on archival and recently measured well data to investigate the groundwater flow direction, i.e., prove the upward flow conditions in the area, which may explain the existence of the springs. The main ions and stable isotopes report on the geochemistry and rock–water interactions, the continuous-time series of water level, temperature, and electrical conductivity data of the springwater reflect the dynamics of the flow system. Finally, the possibility of that scenario, in which the Villány Hills infiltrated meteoric water can be heated up and discharge in Kistapolca with elevated temperature, was tested by numerical simulation.

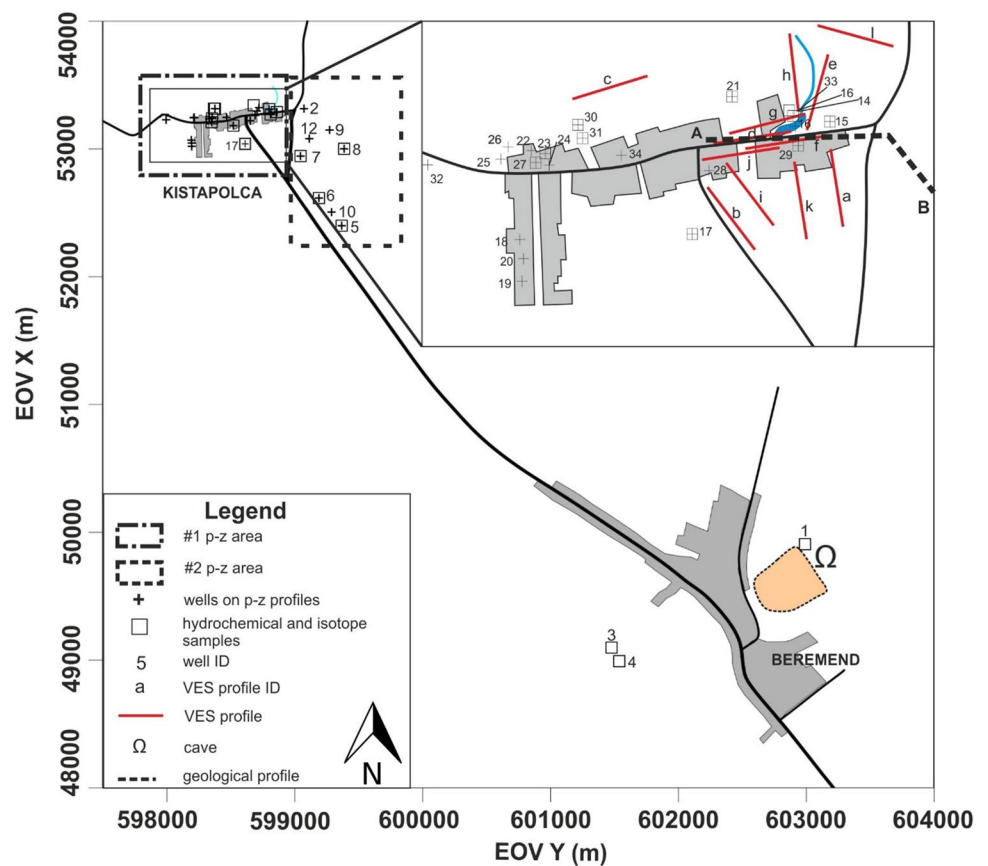
## Geophysical investigation

The aim of the geophysical measurements was to map the surface of the uplifted carbonate basement block in detail, identify the thickness of the cover sediments and the structural elements. Previous geoelectrical measurements by Rónaki et al. (1967) and Deák et al. (1969) provided only a rough overview of the area. Vertical electrical soundings (VES) is often used to determine the depth and thickness of different geological units or the fracture distribution. In this study, VES using Schlumberger array was carried out at 10 VES stations around the lake in Kistapolca (Fig. 3), with the current electrode spacing of  $AB/2 = 70$  M. From the apparent resistivity values ( $\rho_a$ ) of VES, the subsurface resistivity distribution was calculated with the help of two computer programs: PISE4 (Geophysical Department of the Université VI of Paris; Gabalda and Tabbagh 1994) and VES (Department of Geophysics, Eötvös Loránd University, Salát and Drahos 2004). In this way, the layer thickness and resistivity values were obtained. The measurements were supplemented by stratigraphic information of nearby boreholes.

## Hydraulic data evaluation: pressure–elevation profiles

Mádl-Szőnyi and Tóth (2015) proved that the gravity-driven regional groundwater flow concept (GDRGF concept) is also applicable in karst regions based on the principle of hydraulic continuity. Therefore, this concept and its methodology were applied here as a working tool. Accordingly, archival and recently measured hydraulic data of the wells were analyzed by one of the basic regional hydraulic methods of hydrogeology, using pressure–elevation [ $p(z)$ ] profiles (Tóth 2009). The main goal was to determine the regime characteristic of the Kistapolca area and the direction of groundwater flow, i.e., downward, horizontal or upward. The required data (well coordinates, wellhead elevation, depth of the static water level, the elevation of the screened interval) for this hydraulic data analysis were collected from archival well documentations and from recent measurements and summarized in Table 1.

**Fig. 3** Detailed map of the study area showing the bounding areas pressure–elevation profiles, the location of the wells involved in pressure–elevation profiles, the location of the hydrogeochemical and isotope sampling sites, the location of vertical electrical sounding (VES) profiles, the Beremend Cave, and the location of A–B profile in Fig. 4



During the hydraulic calculations, measured hydraulic head data were converted to pore-pressure values with the help of the following equation, which assumes constant fluid density along the flow path:

$$h = z + p/(\rho \times g)$$

where  $h$  is the measured hydraulic head;  $z$  is the elevation of the measuring point with respect to the Baltic Sea level;  $p$  is pore pressure;  $(\rho \times g)$  is the specific weight of the fluid, which is numerically equal to the hydrostatic vertical pressure gradient of that fluid. Pore-pressure data and the hydrostatic vertical pressure gradient [9.81 MPa km<sup>-1</sup>] indicated on the  $p(z)$  profiles were determined by applying the water density of 1000 kg m<sup>-3</sup>.

The  $p(z)$  profiles allow for the examination of the vertical component of fluid flow directions by comparing the vertical pressure gradient to the ideal hydrostatic condition. The vertical pressure gradient ( $\gamma$ ) is the change in pore pressure per unit vertical length in a flow domain. Ideally, in the hydrostatic condition, there is no vertical fluid flow because the buoyancy and the force of gravity on water particles are in balance. In this case, the vertical pressure gradient is hydrostatic, and its average value is  $\gamma_{st} = 9.81 \text{ MPa km}^{-1}$ , by applying the water density of 1000 kg m<sup>-3</sup>. In the hydrodynamic

state, a driving force can shift the system off balance, therefore the vertical flow component occurs too, and the vertical pressure gradient changes to dynamic ( $\gamma_{dyn}$ ). In recharge areas  $\gamma_{dyn} < \gamma_{st}$ , so there is a downward flow direction and  $\gamma_{dyn}$  is called subhydrostatic, while in discharge areas  $\gamma_{dyn} > \gamma_{st}$ , thus there is an upward flow direction and  $\gamma_{dyn}$  is called super-hydrostatic. In midline areas, the vertical pressure gradient is hydrostatic ( $\gamma_{dyn} = \gamma_{st}$ ); therefore, the fluid flow has no vertical component; nevertheless, the horizontal component cannot be excluded. Wells interpreted in one  $p(z)$  profile had to have approximately the same land surface elevation, because the position of the reference hydrostatic pressure gradient line depends on it.

### Hydrogeochemical investigation including stable isotopes

For hydrogeochemical and stable isotope investigations, 17 water samples were collected from dug wells, operating drilled wells, from the mainspring in Kistapolca and from the Beremend Cave at the same time (28–30 August, 2017). Water samples for stable isotope measurements were repeatedly collected from the Beremend Cave (4 samples) and from the mainspring in Kistapolca (2 samples), however, the temporal variation of the measured values were

**Table 1** Well data used for the construction of pressure–elevation profiles in Fig. 5

| #  | p–z# | EOV X  | EOV Y   | z     | h    | p    | T [°C] | Lithology       |
|----|------|--------|---------|-------|------|------|--------|-----------------|
| 2  | 2    | 53,316 | 599,070 | −28.9 | 95.9 | 1.22 | –      | Carbonate       |
| 5  | 2    | 52,399 | 599,365 | 71.6  | 93.5 | 0.21 | 15.2   | Cover sediments |
| 6  | 2    | 52,614 | 599,190 | 67.5  | 91.5 | 0.2  | 19.9   | Cover sediments |
| 7  | 2    | 52,945 | 599,047 | −25.3 | 96.6 | 1.20 | 23.6   | Carbonate       |
| 8  | 2    | 53,001 | 599,387 | −75.0 | 84.4 | 1.56 | 15.8   | Carbonate       |
| 9  | 2    | 53,148 | 599,273 | −20.5 | 96.6 | 1.15 | –      | Carbonate       |
| 10 | 2    | 52,505 | 599,288 | 70.1  | 93.7 | 0.23 | –      | Cover sediments |
| 11 | 2    | 52,614 | 599,190 | 67.5  | 91.5 | 0.24 | –      | Cover sediments |
| 12 | 2    | 53,081 | 599,114 | −8.3  | 96.4 | 1.03 | –      | Carbonate       |
| 13 | 2    | 53,081 | 599,114 | −8.2  | 96.4 | 1.03 | –      | Carbonate       |
| 14 | 1    | 53,313 | 598,798 | 94.3  | 94.7 | 0.00 | 23.7   | Carbonate       |
| 15 | 1    | 53,288 | 598,859 | 85.0  | 90.5 | 0.05 | 17.2   | Cover sediments |
| 16 | 1    | 53,321 | 598,720 | 95.0  | 96.0 | 0.01 | –      | Carbonate       |
| 17 | 1    | 53,181 | 598,519 | 68.3  | 96.9 | 0.28 | 23.7   | Carbonate       |
| 18 | 1    | 53,070 | 598,192 | 73.7  | 89.4 | 0.15 | –      | Cover sediments |
| 19 | 1    | 53,018 | 598,195 | 87.9  | 89.1 | 0.01 | 15.8   | Cover sediments |
| 20 | 1    | 53,046 | 598,194 | 86.6  | 88.7 | 0.02 | –      | Cover sediments |
| 21 | 1    | 53,262 | 598,689 | 91.3  | 97.5 | 0.06 | 20.5   | Cover sediments |
| 22 | 1    | 53,238 | 598,354 | 89.4  | 90.7 | 0.01 | –      | Cover sediments |
| 23 | 1    | 53,246 | 598,351 | 69.1  | 90.1 | 0.21 | 26.1   | Cover sediments |
| 24 | 1    | 53,236 | 598,329 | 88.8  | 91.1 | 0.02 | 17.6   | Cover sediments |
| 25 | 1    | 53,244 | 598,211 | 90.2  | 93.2 | 0.03 | 15.9   | Cover sediments |
| 26 | 1    | 53,248 | 598,213 | 89.0  | 92.9 | 0.04 | 16.6   | Cover sediments |
| 27 | 1    | 53,208 | 598,348 | 84.9  | 87.6 | 0.03 | 20.7   | Cover sediments |
| 28 | 1    | 53,221 | 598,651 | 88.4  | 88.8 | 0.00 | 20.1   | Cover sediments |
| 29 | 1    | 53,268 | 598,811 | 91.7  | 92.2 | 0.00 | 16.5   | Cover sediments |
| 30 | 1    | 53,314 | 598,375 | 85.9  | 90.4 | 0.04 | 21.8   | Cover sediments |
| 32 | 1    | 53,229 | 597,995 | 53.3  | 94.7 | 0.41 | 15.2   | Carbonate       |
| 33 | 1    | 53,295 | 598,706 | 92.5  | 96.3 | 0.04 | 19.5   | Cover sediments |
| 34 | 1    | 53,247 | 598,467 | 95.6  | 96.7 | 0.01 | 21.7   | Cover sediments |

The table includes measured temperature values shown in Fig. 7

not evaluated during this study, due to the small number of samples. Temperature and electrical conductivity were recorded on the field by YSI ProPlus. Among the main ions  $\text{Ca}^{2+}$ ,  $\text{Mg}^{2+}$ ,  $\text{HCO}_3^-$  were analyzed by acid–base titrimetry,  $\text{Cl}^-$  by complexometric titration,  $\text{Na}^+$  and  $\text{K}^+$  were detected by flame photometry and  $\text{SO}_4^{2-}$  by photometry at the Department of Geology of Eötvös Loránd University.

The major components of the water samples were investigated and illustrated on Piper diagram. Piper diagrams represent the main anion and cation compositions in the percentage of the total equivalents per liter. The waters are also classified using the hydrochemical facies concept of Back (1966), which is also illustrated on the Piper diagram. Based on the dominant anion and cation, the  $\text{Ca} + \text{Mg}/\text{HCO}_3$  ratio was calculated in order to evaluate their origin.

Stable hydrogen and oxygen isotope measurements of groundwater were determined at the Institute for Geological and Geochemical Research in Budapest using the liquid

water isotope analyzer, manufactured by Los Gatos Research Ltd. (LWIA-24d). The instrument uses an off-axis integrated cavity ring-down spectroscopy to measure the absolute abundances of  $^2\text{H}^1\text{H}^{16}\text{O}$ ,  $^1\text{H}^1\text{H}^{18}\text{O}$ , and  $^1\text{H}^1\text{H}^{16}\text{O}$  via laser absorption (Lis et al. 2008). Thus, the  $\delta^2\text{H}$  and  $\delta^{18}\text{O}$  values were determined simultaneously and expressed relative to VSMOW standard in ‰. Standardization was conducted using laboratory standard water samples that were calibrated by the international standards (Czuppon et al. 2018). The precisions are better than  $\pm 1.0\text{‰}$  and  $\pm 0.15\text{‰}$  for hydrogen and oxygen, respectively.

### Continuously recorded data

A Dataqua continuous measuring device recorded the change in water level, temperature, and electrical conductivity values in every 6 hours in the captured main-spring in Kistapolca (accuracy:  $\pm 0.1\text{ °C}$ , EC ref.  $20\text{ °C}$ ,

accuracy  $\pm 1\%$ ). The daily precipitation data were obtained from the meteorological station in Nagyharsány (Fig. 1) and were compared with the water level, temperature and electrical conductivity changes in the mainspring.

## Numerical simulation

Numerical simulation of groundwater flow and heat transport were performed to establish a hydrogeologic conceptual model depicting and confirming the groundwater flow directions and processes in the vicinity of the lukewarm spring. The 2D numerical model was built in COMSOL Multiphysics 5.1. applying the fluid flow/porous media and subsurface flow/Darcy's law and heat transfer/heat transfer in porous media modules operating with the finite element numerical approach (Zimmerman 2006). During the calculations, Darcy's equation and the Fourier–Kirchhoff equation were coupled and solved without source/sink, the fluid was incompressible and isothermic, and gravitational acceleration and dynamic viscosity were kept as constant. The study was stationary because of the relatively shallow (thickness:  $\sim 300$  m, length: 17 km) model domain and thus the temperature difference between the boundaries, presumably the water table variation (large hydraulic head gradient) is the main driving force of fluid flow demonstrated by Szijártó et al. (2019). Consequently, only conduction and advection (forced convection) were taken into account.

The boundary conditions were determined on the basis of measured hydraulic and temperature data of wells and they are shown in Fig. 3. Hydraulic head values were specified along the boundaries, on the upper boundary hydraulic head changes from point to point according to the observed water

table. The upper condition for heat transport is the annual mean air temperature ( $11\text{ }^{\circ}\text{C}$ ), while the lower temperature was  $22\text{ }^{\circ}\text{C}$  with respect to measured water temperature. Symmetry type boundary conditions were applied on the side borders meaning that there is no heat flux across the boundary.

The model consists of two main hydrostratigraphic units: surface siliciclastic confining layer and thick carbonates (the bottom of this unit is unknown) and five numerical domains. Regarding the hydraulic conductivity, one order of anisotropy was applied (the horizontal one is 10 times higher than the vertical hydraulic conductivity). The hydraulic (porosity and hydraulic conductivity) properties and the thermal conductivity of the units were determined on the basis of analogs and literature references (Mádl-Szőnyi and Tóth 2015; Freeze and Cherry 1979; Brassington 2017; Beardmore and Cull 2001; Clark 1966).

## Results

### Geophysical measurements

Based on the VES measurements and stratigraphic data of boreholes, the position of the carbonate basement block was refined (Fig. 4), compared to the results of the geophysical survey in the 1960s (Rónaki et al. 1967). The sedimentary cover layers of carbonates are characterized by  $7\text{--}51\ \Omega\text{m}$  apparent resistivity values, whereas the carbonate basement's apparent resistivity values vary between  $175$  and  $700\ \Omega\text{m}$ . Thus, the basement carbonates can be clearly separated from the cover sediments by this

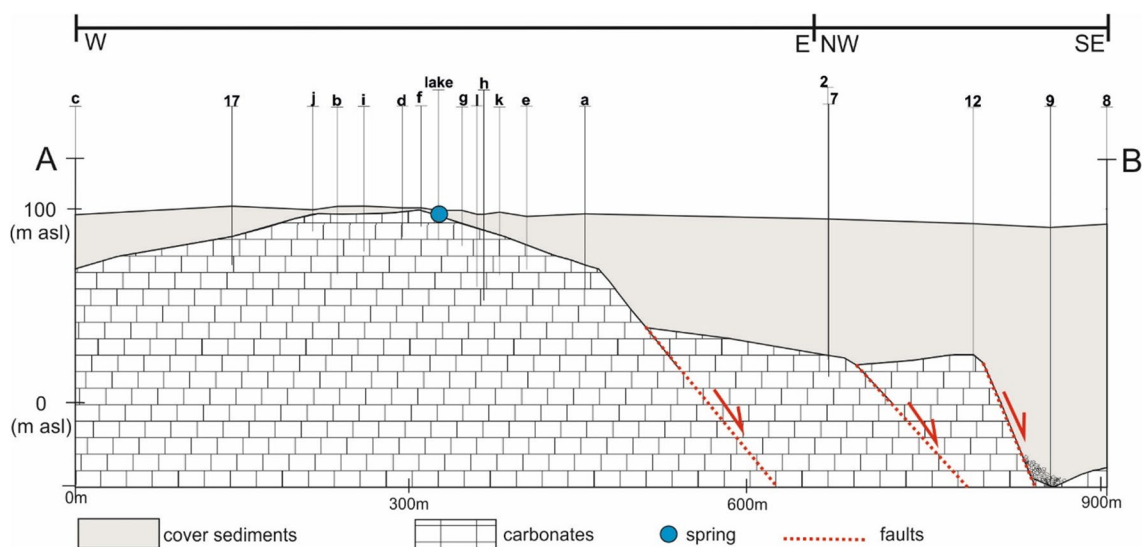


**Fig. 4** A-B simplified geological profile through Kistapolca (see location in Fig. 3) based on the results of vertical electrical soundings and borehole stratigraphic data showing the situation of the carbonate basement under the sediment cover

method. The depth of the carbonate basement, i.e., the sediment cover thickness, varies between 1 and 130 m in the Kistapolca area. The basement situated in the highest position, i.e., closest to the surface in the close vicinity of the lake. The carbonate rock surface sharply deepens to the east, southeast from the lake (up to 130 m in borehole Nr 9., Fig. 4); therefore, structural elements (faults) can be hypothesized. To the west, the depth of the carbonate basement increases evenly and reaches 40 m at the edge of the village (borehole Nr 32., Fig. 3).

### Pressure–elevation profiles

Two  $p(z)$  profiles were constructed in order to evaluate the vertical flow directions (Fig. 5). The area of  $p(z)$  profile #1 is located in the village of Kistapolca (Fig. 3). The data of dug and drilled wells represent the 53.29–95.63 m asl elevation ( $z$ ) interval (Table 1). The vertical pressure gradient is greater than the hydrostatic ( $\gamma_{st} = 9.81 \text{ MPa km}^{-1}$ ), i.e., super-hydrostatic ( $\gamma_{dyn} = 10.45 \text{ MPa km}^{-1}$ ) and refers to the upward vertical flow direction (Fig. 5). The area of  $p(z)$  profile #2 is located in SE vicinity of the settlement (Fig. 3). The profile was compiled based on the wells of the cement factory and represent a wider elevation interval, between (–74.96)–71.55 m asl (Table 1). A slightly smaller than hydrostatic, i.e., subhydrostatic vertical pressure gradient ( $\gamma_{dyn} = 9.74 \text{ MPa km}^{-1}$ ) could be inferred, which refers rather to hydrostatic conditions (Fig. 5). That means that in this area horizontal flow is dominant, the water flow has no vertical component.

### Hydrogeochemistry

Using the main cations and anions, the geochemical facies (Back 1966) was determined and with the help of the Piper diagram it was illustrated (Fig. 6). The  $\text{HCO}_3$ ,  $\text{Cl} + \text{SO}_4$  anion facies with dominating bicarbonate anion is prevalent in the area. Regarding cation facies the waters can be divided into two groups:  $\text{Ca} + \text{Mg}$  cation facies and  $\text{Ca} + \text{Mg}$ ,  $\text{Na} + \text{K}$  cation facies occur in the area. In the majority of the samples, calcium ion is dominating, in two cases magnesium dominance is observed (Nr. 1 and Nr. 5 in Table 2). According to the dominant  $\text{Ca} + \text{Mg}$  cation and  $\text{HCO}_3$  anion their ratio was calculated (Table 2), which is close to one, except the two magnesium dominating sampling sites (Nr. 1 and Nr. 5).

The onsite recorded temperature of the water samples varies between 14 and 26 °C. There is a pattern regarding the spatial distribution of temperature data (Fig. 7). In the eastern part of the village, temperatures are higher than 20 °C, while in the western part values around 16 °C occur. The electrical conductivity values, which refer to the dissolved solid content of the waters, vary between 425 and 1361  $\mu\text{S/cm}$  (Table 2). The lowest value was measured in the Beremend Cave as 425  $\mu\text{S/cm}$  (Nr. 1 in Table 2). The highest values were measured in dug wells in Kistapolca (Nr. 15, 27 in Table 2).

### Stable isotopes

The  $\delta\text{D}$  and  $\delta^{18}\text{O}$  values of the studied wells, springwater, and the waters from Beremend Cave show relative large variation, and they are plotted close to the local meteoric

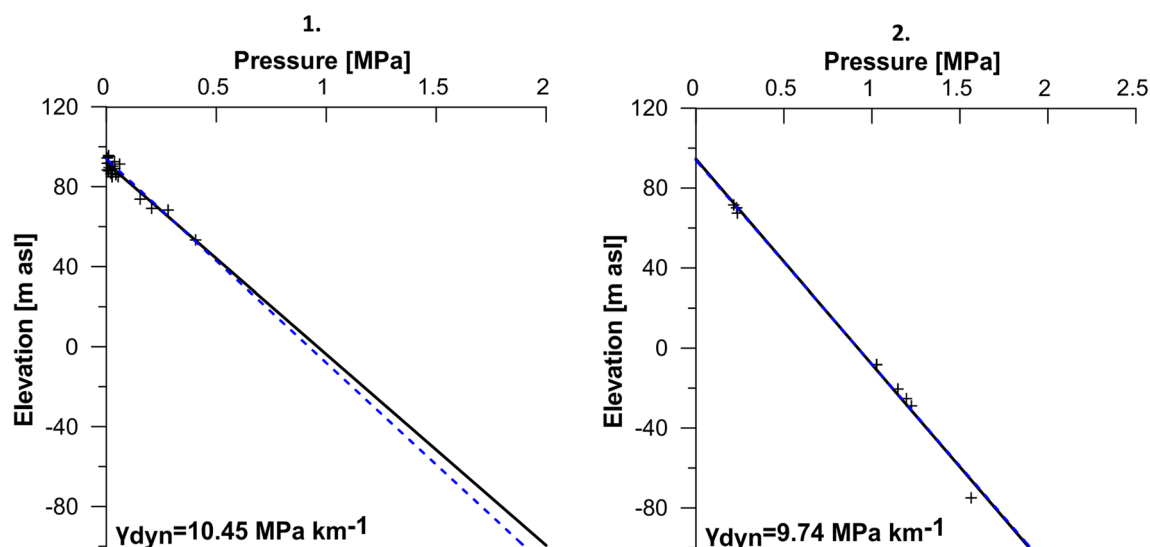
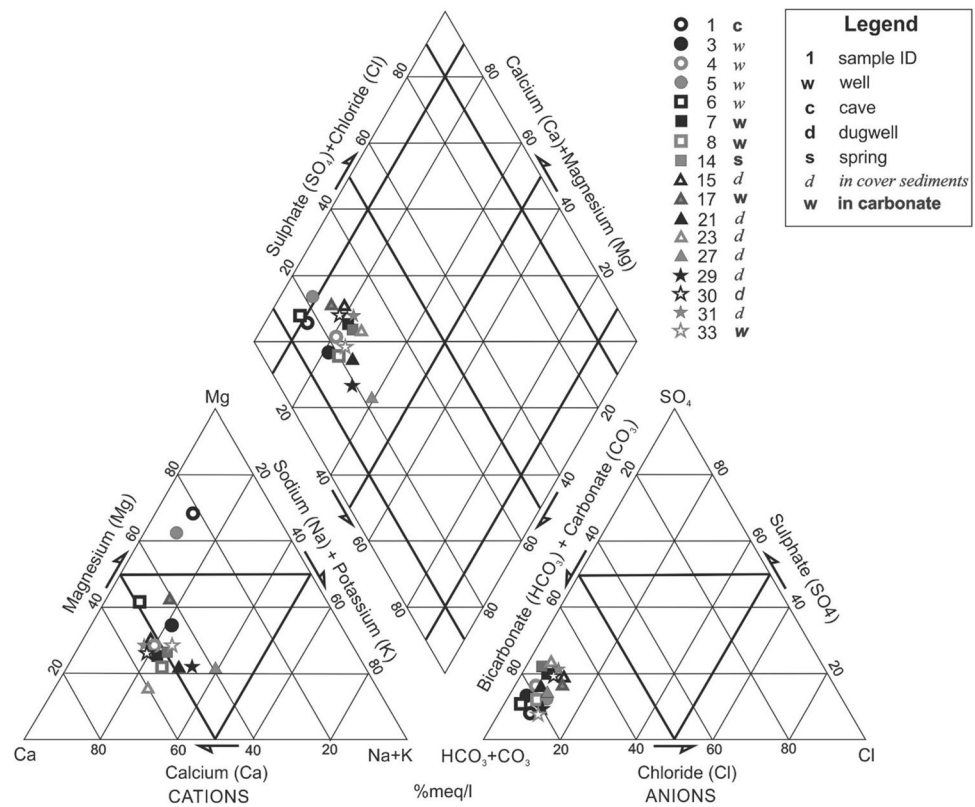


**Fig. 5** Pressure–elevation profiles #1 and #2 constructed based on archival and recently measured well data (Table 1). Hydrostatic vertical pressure gradient [ $9.81 \text{ MPa km}^{-1}$ ] indicated on the  $p(z)$  profiles by dashed lines



**Fig. 6** Piper diagram of the sampled waters (data in Table 2, the location of the sampled wells in Fig. 3)



water line (LMWL defined by Czappon et al. 2017) (Fig. 8). All values are lower than the composition of the amount weighted average of annual precipitation. The water from Beremend Cave (Nr. 1) is characterized by the most positive values ( $\delta D \approx -64.0\text{‰}$  and  $\delta^{18}O \approx -8.9\text{‰}$ ) (Table 2), while the most negative stable isotope composition ( $\delta D \approx -77.9\text{‰}$  and  $\delta^{18}O \approx -10.9\text{‰}$ ) were found in the Kistapolca springwater (Nr. 14) and some drilled and dug wells (Nr. 7, 8, 17, 21, 30, 31) in Kistapolca. The other studied wells show intermediate values between these “endmembers”. Interestingly, these dug wells (Nr. 21, 30, 31) in Kistapolca are constructed in the cover sediments, which show similar negative isotopic composition to those wells producing waters from the carbonate aquifer (Nr. 7, 8, 17) and also similar to the springwater (Nr. 14). Water sample from the Beremend Cave (Nr. 1), however, shows similarities to those wells which are producing waters from the sedimentary cover of the carbonate aquifer (Nr. 3, 5, 6, 15).

**Continuously recorded data**

The data of continuous measurement device in the captured main spring show that both the temperature (22.4–23.5 °C) and electrical conductivity values (890–911  $\mu\text{S}/\text{cm}$ ) are rather stable in the observed half-year period. The observed variation of the temperature is within 1 °C and the observed variation of the electrical conductivity values is maximum 20  $\mu\text{S}/\text{cm}$ .

Both can be considered rather stable. Effects of precipitation periods, however, can be visually recognized in water level increase (Fig. 9).

**Numerical modeling**

The outcropping carbonates function as recharge areas, where the groundwater is replenished and intense, mostly downward-oriented flow occurred. The magnitude of groundwater flow (color scale) was 1–2 orders less in the confined carbonate and the confining bed itself Fig. 10. The direction of water movement is represented by normalized uniform flow vectors, which showed a convergence zone and a discharge area under the village of Kistapolca in the carbonate dome. The spring received groundwater both from the Northern and Southern parts. The infiltrating cold meteoric water transported by advection penetrated down to the bottom of the model geometry. However, the lukewarm groundwater could rise and reach the surface. Under and within the siliciclastic confining layer, the groundwater could be heated up and 15–20 °C of temperature could be expected and observed.

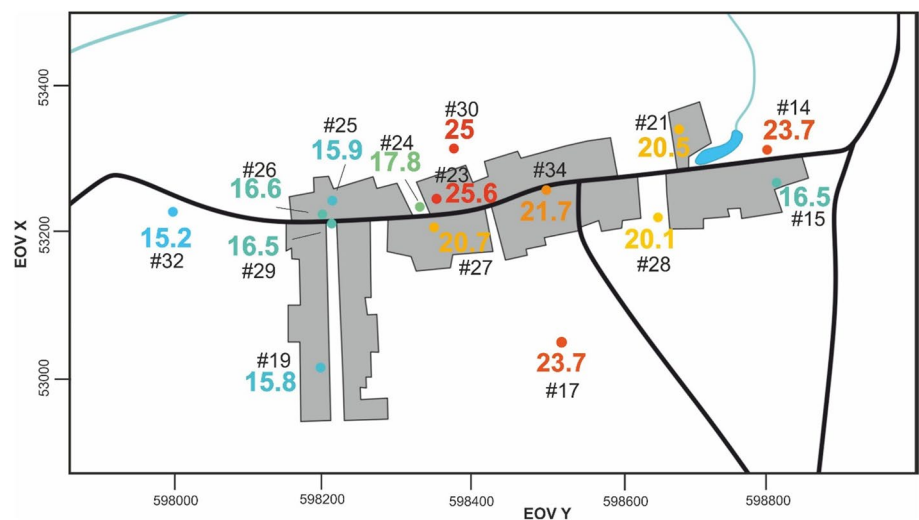
**Table 2** Temperature, electrical conductivity, main anions and cations, and stable isotope data of the sampled waters

| #  | Temp. [°C] | EC [ $\mu\text{S cm}^{-1}$ ] | $\text{HCO}_3^-$ [ $\text{mg L}^{-1}$ ] | $\text{Ca}^{2+}$ [ $\text{mg L}^{-1}$ ] | $\text{Mg}^{2+}$ [ $\text{mg L}^{-1}$ ] | $\text{Cl}^-$ [ $\text{mg L}^{-1}$ ] | $\text{SO}_4^{2-}$ [ $\text{mg L}^{-1}$ ] | $\text{K}^+$ [ $\text{mg L}^{-1}$ ] | $\text{Na}^+$ [ $\text{mg L}^{-1}$ ] | TDS [ $\text{mg L}^{-1}$ ] | Ca+Mg/<br>$\text{HCO}_3$ | dD       | $\text{d}^{18}\text{O}$ |
|----|------------|------------------------------|---|---|---|--------------------------------------|---|-------------------------------------|--------------------------------------|----------------------------|--------------------------|----------|-------------------------|
| 1  | 18.1       | 425                          | 300                                     | 53                                      | 102                                     | 15                                   | 26  | 3                                   | 23                                   | 522.0                      | 2.26                     | -64.07*  | -8.94*                  |
| 3  | 13.9       | 722                          | 468                                     | 83                                      | 40                                      | 14                                   | 62  | 21                                  | 31                                   | 718.5                      | 0.97                     | -68.73   | -9.59                   |
| 4  | 14.2       | 855                          | 493                                     | 98                                      | 33                                      | 20                                   | 83  | 5                                   | 40                                   | 772.0                      | 0.95                     | -73.76   | -10.30                  |
| 5  | 15.2       | 652                          | 378                                     | 61                                      | 80                                      | 26                                   | 51  | 1                                   | 18                                   | 614.7                      | 1.57                     | -66.22   | -9.28                   |
| 6  | 19.9       | 772                          | 449                                     | 89                                      | 46                                      | 16                                   | 49  | 1                                   | 17                                   | 667.6                      | 1.13                     | -65.44   | -9.21                   |
| 7  | 23.6       | 962                          | 536                                     | 111                                     | 33                                      | 26                                   | 124                                       | 10                                  | 45                                   | 885.1                      | 0.95                     | -77.97   | -10.88                  |
| 8  | 15.8       | 950                          | 549                                     | 102                                     | 29                                      | 26                                   | 74  | 8                                   | 47                                   | 835.5                      | 0.84                     | -78.40   | -10.82                  |
| 14 | 23.7       | 968                          | 524                                     | 107                                     | 34                                      | 26                                   | 119                                       | 9                                   | 48                                   | 867.1                      | 0.95                     | -77.78** | -10.73**                |
| 15 | 17.2       | 1361                         | 686                                     | 153                                     | 56                                      | 47                                   | 152                                       | 42                                  | 36                                   | 1171.4                     | 1.09                     | -68.32   | -9.59                   |
| 17 | 23.7       | 968                          | 536                                     | 104                                     | 70                                      | 36                                   | 102                                       | 9                                   | 44                                   | 900.5                      | 1.25                     | -77.46   | -10.82                  |
| 21 | 20.5       | 982                          | 518                                     | 111                                     | 34                                      | 25                                   | 89  | 8                                   | 68                                   | 853.0                      | 0.99                     | -77.55   | -10.74                  |
| 23 | 26.1       | 975                          | 511                                     | 111                                     | 19                                      | 25                                   | 125                                       | 10                                  | 44                                   | 844.6                      | 0.85                     | -76.86   | -10.68                  |
| 27 | 20.7       | 1268                         | 492                                     | 96                                      | 33                                      | 31                                   | 72  | 62                                  | 72                                   | 857.7                      | 0.94                     | -73.34   | -10.24                  |
| 29 | 16.5       | 1065                         | 543                                     | 113                                     | 34                                      | 31                                   | 58  | 41                                  | 65                                   | 884.7                      | 0.95                     | -76.00   | -10.63                  |
| 30 | 21.8       | 966                          | 518                                     | 109                                     | 34                                      | 24                                   | 115                                       | 10                                  | 46                                   | 856.3                      | 0.98                     | -77.95   | -10.83                  |
| 31 | 25.1       | 969                          | 518                                     | 115                                     | 34                                      | 24                                   | 124                                       | 10                                  | 45                                   | 870.8                      | 1.02                     | -77.86   | -10.83                  |
| 33 | 19.5       | 849                          | 424                                     | 87                                      | 32                                      | 25                                   | 62  | 21                                  | 31                                   | 681.8                      | 1.01                     | -72.79   | -9.84                   |

\* Average value of four repeated measurements ( $\delta\text{D}$ : -64.28,  $\delta^{18}\text{O}$ : -9.08 (28.08.2017);  $\delta\text{D}$ : -63.84,  $\delta^{18}\text{O}$ : -8.90 (09.03.2018);  $\delta\text{D}$ : -63.75,  $\delta^{18}\text{O}$ : -8.88 (10.10.2018);  $\delta\text{D}$ : -64.42,  $\delta^{18}\text{O}$ : -8.92 (03.05.2019))

\*\* Average value of two repeated measurements ( $\delta\text{D}$ : -77.76,  $\delta^{18}\text{O}$ : -10.79 (28.08.2017);  $\delta\text{D}$ : -77.81,  $\delta^{18}\text{O}$ : -10.69 (03.05.2019))

**Fig. 7** Temperature distribution in the sampled wells (data in Table 1 and Table 2)



**Discussion**

Based on the VES measurements and stratigraphic data of boreholes, the position of the carbonate basement block was refined in Kistapolca (Fig. 4) compared to the results of the geophysical survey in the 1960s (Rónaki et al. 1967). The results show that the basement situated in the highest position, i.e., closest to the surface in the close vicinity of the lake, which explains the existence of the springs. The

pressure–elevation profiles showed greater than the hydrostatic ( $\gamma_{dyn} = 10.45 \text{ MPa km}^{-1}$ ), i.e., super-hydrostatic vertical pressure gradient in Kistapolca, which refers to the upward vertical flow direction (Fig. 5). This also supports and explains the existence of springs. This method as part of the gravity-driven regional groundwater flow (GDRGF) concept’s methodology (Tóth 2009) was previously commonly applied only in sedimentary basins. However, recent investigations (Mádl-Szőnyi and Tóth 2015; Erhardt et al. 2017) highlighted its applicability in karst areas. Pressure–elevation profiles were applied by Erhardt et al. (2017) in a similar, marginal karst area, where the springs and discharge areas were verified by this method. The results in Kistapolca further strengthen the applicability of flow system analysis methodology in karst areas.

The VES measurements, the stratigraphic data of boreholes and the spatial distribution of temperature in wells (Fig. 7), suggest the existence of faults within the uplifted basement carbonate block, which can serve as pathways for the upward flow. This upward flow and the discharge effect of karst waters into the cover sediments are also evident from the isotopic composition of dug wells (Nr. 21, 23, 29, 30, 31) and springwater (Nr. 14), that are characterized by low hydrogen and oxygen isotope values ( $\delta D \approx -77.9\text{‰}$  and  $\delta^{18}\text{O} \approx -10.9\text{‰}$ ). This is also reflected by the bicarbonate and calcium dominance in these wells. The  $\text{Ca} + \text{Mg}/\text{HCO}_3$  ratio is close to 1 also implying carbonate dissolution-related origin of these waters (Zaidi et al. 2015). Higher (1268–1361  $\mu\text{S}/\text{cm}$ ) electric conductivity values of dug wells (e.g., Nr 15 and 27 in Table 2.) may also indicate anthropogenic influence, which may originate from livestock breeding in the backyard of the houses.

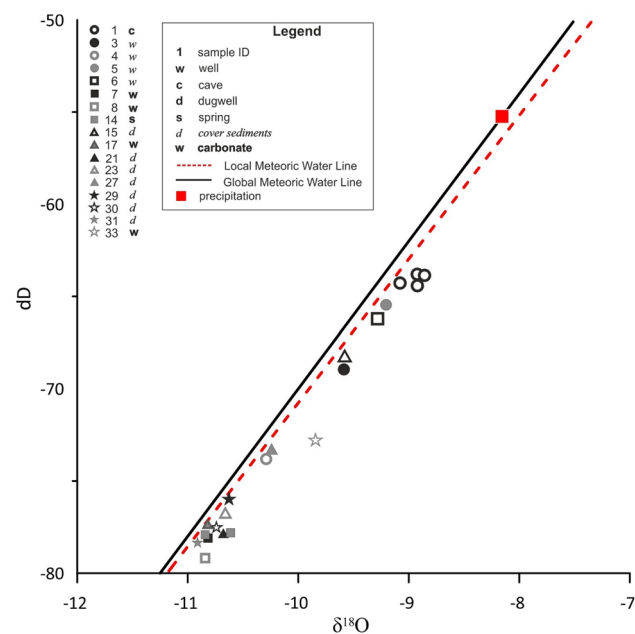
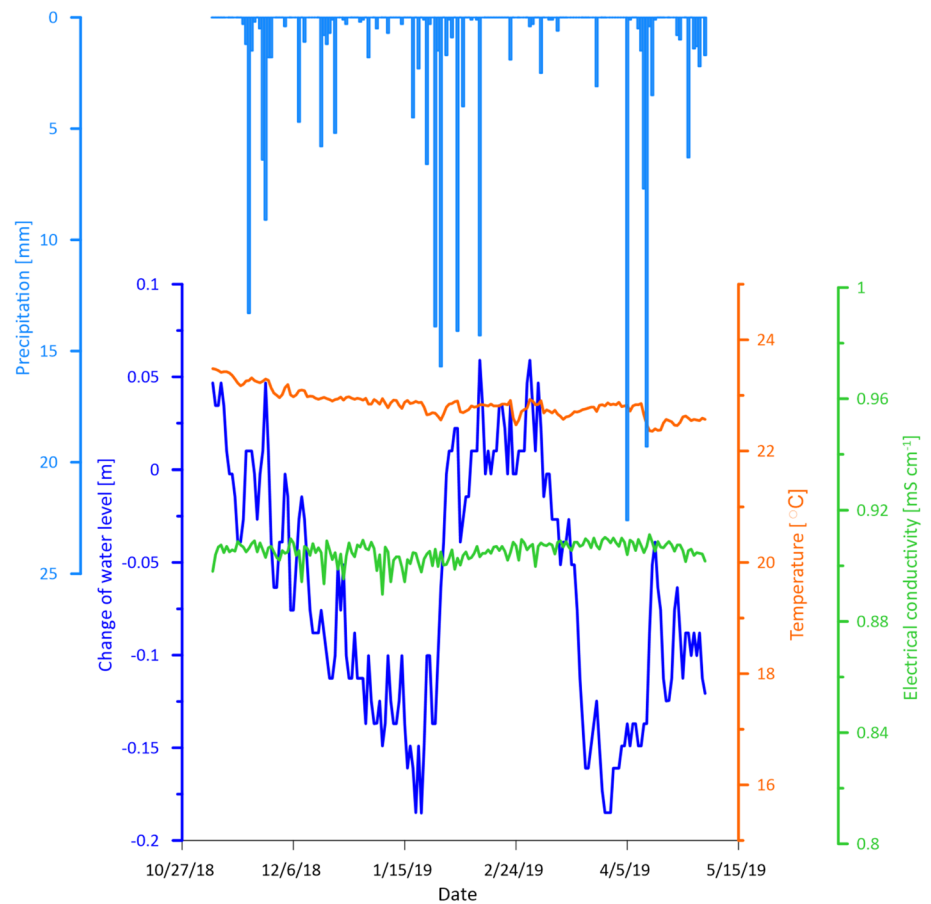


**Fig. 8** Isotopic composition of the sampled waters (data in Table 2). GMWL and LMWL indicates the global meteoric water line and the local meteoric water line (Czuppon et al. 2017), respectively. As a reference, the annual amount weighted isotopic composition of precipitation is also indicated (Czuppon et al. 2017)

The hydraulic characteristics of karst aquifers are very different from other aquifer types, as they hold a complex conduit network (Goldscheider and Drew 2007). Precipitation events may cause sudden water level increase in the

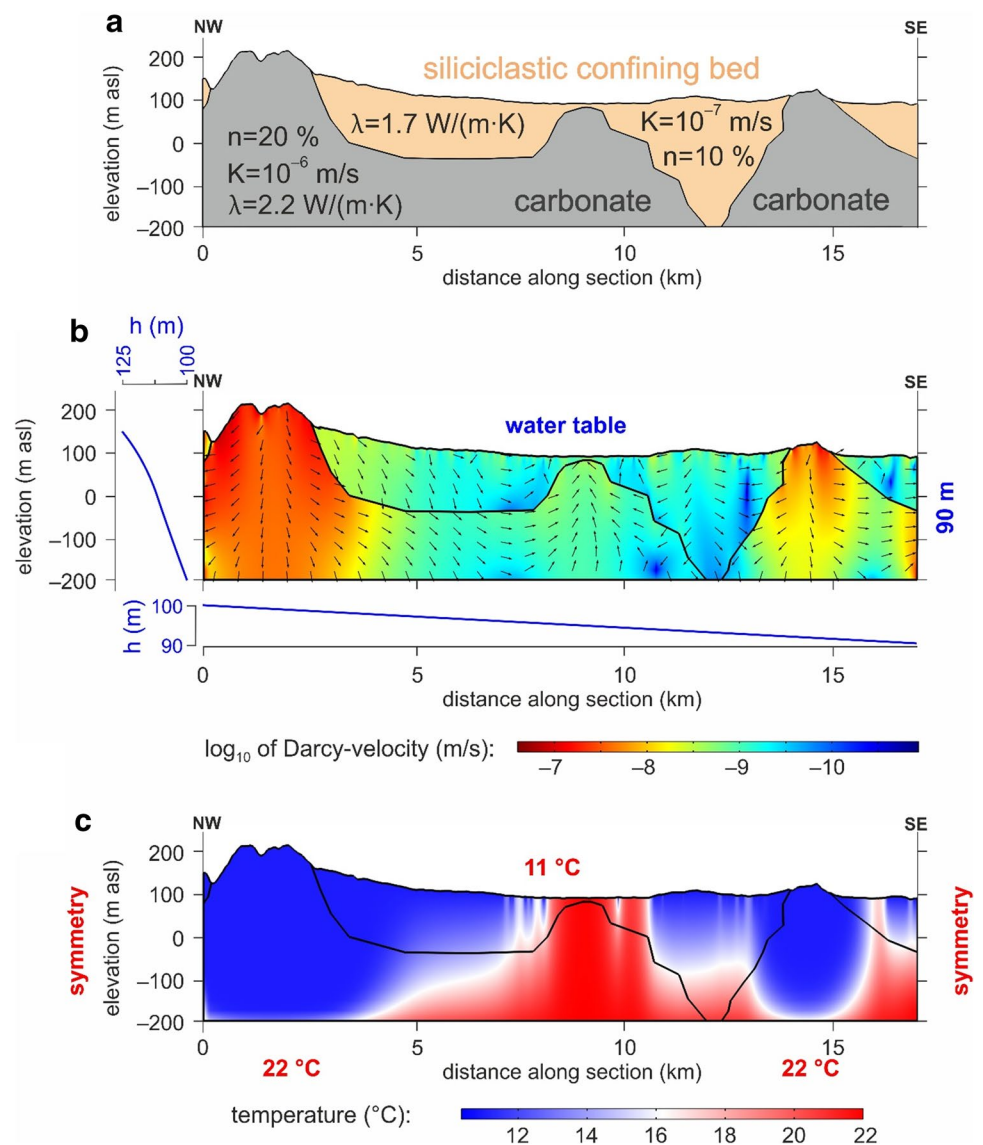
**Fig. 9** Continuously recorded water level change, electric conductivity, and temperature data of the mainspring (lines) and the daily precipitations in Nagyharsány (bars)



system and discharge peak in the springs accompanied by the decrease of electrical conductivity (Király and Müller 1979; Groves 2007). The visually recognizable connection between precipitation events and the water level increase indicates the dynamic response of the thick carbonate reservoir on precipitation in the form of regional water level increase (Fig. 9). The stability of electrical conductivity and temperature over time in the mainspring, however, indicates that local infiltration, local flow system have no direct, immediate effect on the spring's parameters. This is also in accordance with the lowest measured isotopic values of the spring and the wells in Kistapolca, as it is discussed above. This suggests the influence of higher order flow systems rather than the local recharge conditions in the wells and springs of Kistapolca, which is also supported by the numerical simulation. Similarly, Malík et al. (2019) found that the response time of spring discharge to sudden groundwater table rise occurred later at springs with a higher water temperature. However, to draw more detailed interpretation about the hydraulic response of the spring and the thick karst reservoir to precipitation events, monitoring data of several years are needed, which is currently not available, but the monitoring is in progress at the mainspring and in the Beremend Cave. Moreover,

it should be noted that some wells show more positive isotopic values ( $\delta D$ : from  $-73.8$  to  $-65.4\text{‰}$  and  $\delta^{18}O$ : from  $-10.3$  to  $-9.2\text{‰}$ ) than the above-mentioned wells and spring, indicating that in some cases, the influence of local, recent precipitation-related water is more pronounced. The isotopic composition of water samples from the Beremend Cave (Nr. 1) shows the most positive values plotting (Fig. 8) closest to those that is observed in the recent precipitation implying lack or very limited effect of higher order flow systems. The measured  $\delta^{18}O$  value of the water in the cave is in accordance with the measurements ( $\delta^{18}O$ :  $-8.8\text{‰}$ ) of Vigassy et al. (2010). The lowest electrical conductivity value ( $425\ \mu\text{S}/\text{cm}$ , Table 2) together with the isotopic composition closest to the precipitation (Fig. 8) in the water of Beremend Cave support the scenario showing the effects of recharge and local flow conditions. The numerical simulation is also in good agreement with these observations. Similar results were reported from the hypogene caves of Black Hills by Bakalowicz et al (1987), showing the influence of the local infiltrating water recently. It can be concluded that the karst water present in the Beremend Cave nowadays does not show the effect of deep flow systems and thermal waters implying that significant mixing of deep and local waters might

**Fig. 10** Numerical simulation results of groundwater flow and heat transport. **a** Model geometry indicating parameters of siliciclastic confining bed and carbonate: K—hydraulic conductivity, n—porosity,  $\lambda$ —thermal conductivity. **b** The intensity of groundwater flow with the normalized flow vectors and boundary conditions. **c** Temperature distribution and the applied boundary conditions of heat transport



already be inactive as today. However, further detailed study, in the Beremend Cave and surroundings, is needed.

The small scale, 5–10 cm water level changes recorded at the mainspring in Kistapolca might be the effect of the water abstraction of the nearby cement factory and the waterworks in the village, which have together yearly about 120 – 145 – 190 × 10<sup>6</sup> m<sup>3</sup> abstracted water amount in the last 3 years, showing an increasing trend (data provided by the General Directorate of Water). Therefore, the groundwater-dependent ecosystem of the lake fed by the spring can rather suffer from this anthropogenic effect. Climate change, i.e., reduced recharge can further strengthen this effect, as large groundwater abstraction superimposed on regional water level decrease may result in longer and more common dry periods of the lake, as it was theoretically investigated by Havril et al. (2018).

### Conclusion

Several methods were applied in the hydrogeological characterization of the surroundings of Kistapolca, where the only naturally outflowing springs of the region can be found. The combination of geophysical, geochemical, hydraulic methods enabled to deliver explanations to the existence of the springs, and multiple pieces of evidence that the spring is fed by a higher order—possibly intermediate—flow system without or limited influence of local flow system. These findings are also supported by numerical simulation. In addition, the vulnerability of the groundwater-dependent lake ecosystem was evaluated as well. The results related to the Beremend Cave indicate that mixing corrosion is not an active process today, the

cave is rather influenced by local processes, however, these should be evaluated in detail in order to keep the protection of the peculiar thermal water-related mineral assemblages of the cave.

**Acknowledgments** Open access funding provided by Eötvös Loránd University. The National Research, Development and Innovation Office—NKFIH has provided financial support to the research under the grant agreement no. PD 116227. The research was achieved in cooperation with the University of Pécs related to the Grant Nr. 20765–3/2018/FEKUTSTRAT (Institutional Excellence Program of Higher Education No. 3/ “Innovation for sustainable, healthy life and environment”; University of Pécs). The authors are grateful for the help of the mayor of Kistapolca and Mrs. Szép, as well as the colleagues of the local waterworks. Assistance in fieldwork is greatly acknowledged to Judit Godányi and Petra Baják. Special thanks to Ádám Tóth and Márk Szijártó for the help and fruitful discussions during numerical simulations. The contribution of the General Directorate of Water is acknowledged by providing water abstraction data.

**Open Access** This article is licensed under a Creative Commons Attribution 4.0 International License, which permits use, sharing, adaptation, distribution and reproduction in any medium or format, as long as you give appropriate credit to the original author(s) and the source, provide a link to the Creative Commons licence, and indicate if changes were made. The images or other third party material in this article are included in the article’s Creative Commons licence, unless indicated otherwise in a credit line to the material. If material is not included in the article’s Creative Commons licence and your intended use is not permitted by statutory regulation or exceeds the permitted use, you will need to obtain permission directly from the copyright holder. To view a copy of this licence, visit <http://creativecommons.org/licenses/by/4.0/>.

## References

- Back W (1966) Hydrochemical facies and groundwater flow patterns in northern part of Atlantic Coastal Plain. AAPG Bull. <https://doi.org/10.3133/pp498A>
- Bakalowicz MJ, Ford DC, Miller TE, Palmer AN, Palmer MV (1987) Thermal genesis of dissolution caves in the Black Hills, South Dakota. *Geol Soc Am Bull* 99(6):729–738. [https://doi.org/10.1130/0016-7606\(1987\)99%3c729:TGOCDI%3e2.0.CO;2](https://doi.org/10.1130/0016-7606(1987)99%3c729:TGOCDI%3e2.0.CO;2)
- Beardmore G, Cull J (2001) Crustal heat flow. Cambridge University Press, Cambridge
- Bögli A (1964) Mischungskorrosion, ein Beitrag zum Verkarstungsproblem. *Erdkunde* 18(2):83–92. <https://doi.org/10.3112/erdkunde.1964.02.02>
- Bögli A (1980) Karst hydrology and physical speleology. Springer, Berlin. <https://doi.org/10.1007/978-3-642-67669-7>
- Brassington R (2017) Field hydrogeology. Wiley, Chichester
- Clark SP (1966) Handbook of physical constants. Geological Society of America, New York
- Császár G (2002) Urgan formations in Hungary with special reference to the Eastern Alps, the Western Carpathians and the Apuseni Mountains. *Geologica Hungarica series Geologica* 25, p 209
- Csicsák J, Gondár K, Majoros Gy (2008) A harkányi Gyógyfürdő Zrt. tulajdonában lévő harkányi, mattyi és büdöstopolcai vízbázisok állapotértékelése és biztonságba helyezési terve. Smaragd GSH és Mecsekérc Zrt
- Czuppon GY, Bottyán E, Kármán K, Haszpra L, Weidinger T (2017) Significance of the air moisture source on the stable isotope composition of the precipitation in Hungary. EGU General Assembly, Geophysical Research Abstracts
- Czuppon GY, Demény A, Sz L-Ó, Óvari M, Molnár M, Stieber J, Kiss K, Kármán K, Surányi G, Haszpra L (2018) Cave monitoring in the Béke and Baradla Caves (Northeastern Hungary): implications for the conditions for the formation cave carbonates. *Int J Speleol* 47:13–28. <https://doi.org/10.5038/1827-806X.47.1.2110>
- Deák I, Karácsony S, Gy S (1969) Vízföldtani tapasztalatok Beremend környékén. *Hidrológiai Közlöny* 11:503–515
- Dezső J, Sebe K, Horváth G (2004) Villányi-hegység útikalauz (Guidebook of Villány Hills). Speleo Club of Univ, Janus Pannonius, Pécs, p 159
- Dublyansky Y, Michajljow W, Bolner-Takács K, Hromas J, Székely K, Hevesi A, Kraus S (2017) Hypogene Karst in the Tyuya-Muyun and the Kara-Tash Massifs (Kyrgyzstan). In: Klimchouk A, Palmer AN, de Waele J, Auler AS, Audra P (eds) Hypogene karst regions and caves of the world. Springer, Cham, pp 495–507
- Erhardt I, Ötvös V, Erőss A, Czauner B, Simon S, Mádl-Szőnyi J (2017) Hydraulic evaluation of the hypogenic karst area in Budapest (Hungary). *Hydrogeol J* 25(6):1871–1891. <https://doi.org/10.1007/s10040-017-1591-3>
- Erőss A, Mádl-Szőnyi J, Surbeck H, Horváth Á, Goldscheider N, Csoma AÉ (2012) Radionuclides as natural tracers for the characterization of fluids in regional discharge areas, Buda Thermal Karst, Hungary. *J Hydrol* 426:124–137. <https://doi.org/10.1016/j.jhydrol.2012.01.031>
- Freeze RA, Cherry JA (1979) Groundwater. Prentice-Hall Inc, Englewood Cliffs, p 604
- Gabalda G, Tabbagh J (1994) Note explicative du Programme d’Interprétation de Sondages Electriques (PISE4), Version 4. ORSTOM-CRG-CNRS, France
- Goldscheider N, Drew D (eds) (2007) Methods in karst hydrogeology, IAH Book Series (no. 26th). Taylor and Francis Group, London
- Groves C (2007) Hydrological methods. In: Goldscheider N, Drew D (eds) Methods in Karst Hydrogeology, IAH Book Series (no. 26th). Taylor and Francis Group, London, pp 45–64
- Havril T, Tóth Á, Molson JW, Galsa A, Mádl-Szőnyi J (2018) Impacts of predicted climate change on groundwater flow systems: Can wetlands disappear due to recharge reduction? *J Hydrol* 563:1169–1180. <https://doi.org/10.1016/j.jhydrol.2017.09.020>
- Kessler H (1959) Az Országos Forrányilvántartás. VITUKI, Budapest, p 104
- Király L, Müller I (1979) Hétérogénéité de la perméabilité et de l’alimentation dans le karst: effet sur la variation du chimisme des sources karstiques. *Bulletin du Centre d’hydrogéologie* 3:237–285
- Klimchouk A (2007) Hypogene speleogenesis: hydrogeological and morphogenetic perspective. Special Paper no. 1. National Cave and Karst Research Institute, Carlsbad
- Klimchouk A (2012) Speleogenesis, hypogenic. In: Klimchouk A, White WB, Culver DC (eds) Encyclopedia of caves. Academic Press, New York, pp 748–765
- Konrád GY, Sebe K, Halász A, Halmi Á (2010) A Délkelet-Dunántúl földtani fejlődéstörténete—recens analógiák/The major phases in the geological evolution of South-East Transdanubia and their recent analogues. *Földrajzi Közlemények* 134(3):251–266
- Leél-Össy SZ (2017) Caves of the Buda Thermal Karst. In: Klimchouk A, Palmer A, De Waele J, Auler AS, Audra P (eds) Hypogene Karst Regions and Caves of the World. Springer, Cham, pp 279–297
- Liebe P, Lorberer Á (1981) A baranyai termális karsztrendszer hidrogeológiai és termodinamikai jellemzői A Magyar Hidrológiai Társaság II Országos Vándorgyűlése II. kötet: 74–82
- Lis G, Wassenaar L, Hendry M (2008) High-precision laser spectroscopy D/H and 18O/16O measurements of microliter natural water samples. *Anal Chem* 80:287–293. <https://doi.org/10.1021/ac701716q>

- Lorberer Á, Rónaki L (1978) A villányi-hegységi karszt vízföldtani és speleológiai viszonyai. Összefoglaló jelentés, Magyar Karszt- és Barlangkutató Társulat, pp 35–64
- Mádl-Szőnyi J, Tóth Á (2015) Basin-scale conceptual groundwater flow model for an unconfined and confined thick carbonate region. *Hydrogeol J* 23(7):1359–1380. <https://doi.org/10.1007/s10040-015-1274-x>
- Mádl-Szőnyi J, Erőss A, Tóth Á (2017) Fluid Flow Systems and Hypogene Karst of the Transdanubian Range, Hungary—With Special Emphasis on Buda Thermal Karst. In: Klimchouk AB, Palmer AN, De Waele J, Auler AS, Audra P (eds) Hypogene karst regions and caves of the world. Springer, Cham, pp 267–278
- Malík P, Coplák M, Kuvik M, Švasta J (2019) Recharge impulse spreading in Western Carpathian's mountainous fissure–karst aquifer. *Water* 11(4):763. <https://doi.org/10.3390/w11040763>
- Meinzer OE (1923) Outline of ground-water hydrology, with definitions. U. S. Geological Survey. Water-supply Paper 494
- Nagy E, Nagy I (1976) A Villányi-hegység triász képződményei. *Geologica Hungarica series Geologica* 17:113–227
- Palmer AN (ed) (2007) Cave geology. Cave Books, Dayton
- Pentecost A, Jones B, Renaut RW (2003) What is a hot spring? *Can J Earth Sci* 40:1443–1446. <https://doi.org/10.1139/e07-008>
- Petrik A (2009) A villányi-hegységi mezozoos képződmények mikrotektonikai méréseinek értelmezése. *Földtani Közlöny* 139(3):217–236
- Plan L, Pavuza R, Seemann R (2006) Das Nasse Schacht bei Mannersdorf am Leithagebirge, NÖ (2911/21) – eine thermal beeinflusste Höhle am Ostrand des Wiener Beckens. *Die Höhle* 57:30–46
- Plan L, Tschegg C, De Waele J, Spötl C (2012) Corrosion morphology and cave wall alteration in an Alpine sulfuric acid cave (Kraushöhle, Austria). *Geomorphology* 169:45–54. <https://doi.org/10.1016/j.geomorph.2012.04.006>
- Rakusz GY, Strausz L (1953) A Villányi-hegység földtana. *A Magyar Állami Földtani Intézet Évkönyve* 41(2):3–27
- Rónaki L, Szederkényi T, Kassai M (1967) Szakvélemény Kistapolca-Old környékének termásvíz feltárási lehetőségeiről - Pécs, 1967. XII.20, p 20
- Salát P, Drahos D (2004) Quality management for electrical and penetration soundings (VES & EGPS). *Geophysical* 44(3–4):195–212
- Scheuer GY (2012) A hazai egyes lemez-tektonikai szerkezeti egységek karsztos hévizeinek előzetes összehasonlító nyomelem vizsgálata. *Hidrológiai Közlöny* 92(1):1–12
- Spötl C, Dublyansky Y, Meyer M, Mangini A (2009) Identifying low-temperature hydrothermal karst and palaeowaters using stable isotopes: a case study from an alpine cave, Entrische Kirche. *Aust Int J Earth Sci* 98(3):665–676. <https://doi.org/10.1007/s00531-007-0263-2>
- Szijaártó M, Galsa A, Tóth Á, Mádl-Szőnyi J (2019) Numerical investigation of the combined effect of forced and free thermal convection in synthetic groundwater basins. *J Hydrol* 572:364–379. <https://doi.org/10.1016/j.jhydrol.2019.03.003>
- Takács-Bolner K (1985) A Beremendi-kristálybarlang. *Karszt és Barlang*, I–II, pp 3–12
- Takács-Bolner K (2003a) A Beremendi-kristálybarlang. In: Székely K (ed) Magyarország fokozottan védett barlangjai. Mezőgazda Kiadó, Budapest, pp 399–404
- Takács-Bolner K (2003b) Nagyharsányi-kristálybarlang. In: Székely K (ed) Magyarország fokozottan védett barlangjai. Mezőgazda Kiadó, Budapest, pp 404–407
- Tóth J (1971) Groundwater discharge: a common generator of diverse geologic and morphologic phenomena. *Int Assoc Sci Hydrol Bull* 16(1–3):7–24
- Tóth J (2009) Gravitational systems of groundwater flow: theory, evaluation, utilization. Cambridge University Press, Cambridge
- Török Á (1998) A Mecsek-Villányi egység triász képződményeinek rétegtana. In: Bérczi I, Jámor Á (eds) Magyarország geológiai képződményeinek rétegtana. Mol Rt. és a MÁFI kiadványa, Budapest, pp 253–279
- Vadász E (1935) A Mecsek-hegység. Magyar tájak földtani leírása, Magyar Királyi Földtani Intézet, Budapest, p 148
- Vigassy T, Leél-Óssy SZ, Demény A (2010) A Nagyharsányi- és a Beremendi-kristálybarlang és képződményeik genetikai vizsgálata. *Földtani Közlöny* 140(1):73–88
- Zaidi FK, Nazzal Y, Jafri MK, Naeem M, Ahmed I (2015) Reverse ion exchange as a major process controlling the groundwater chemistry in an arid environment: a case study from northwestern Saudi Arabia. *Environ Monit Assess* 187(10):607. <https://doi.org/10.1007/s10661-015-4828-4>
- Zimmerman WB (2006) Multiphysics modeling with finite element methods. World Scientific Publishing Company, London, p 422

**Publisher's Note** Springer Nature remains neutral with regard to jurisdictional claims in published maps and institutional affiliations.